Chapter 5

Patient-Specific Blood Flow and Pressure Modelling of Suspected Coronary Artery Disease Using Open Loop System

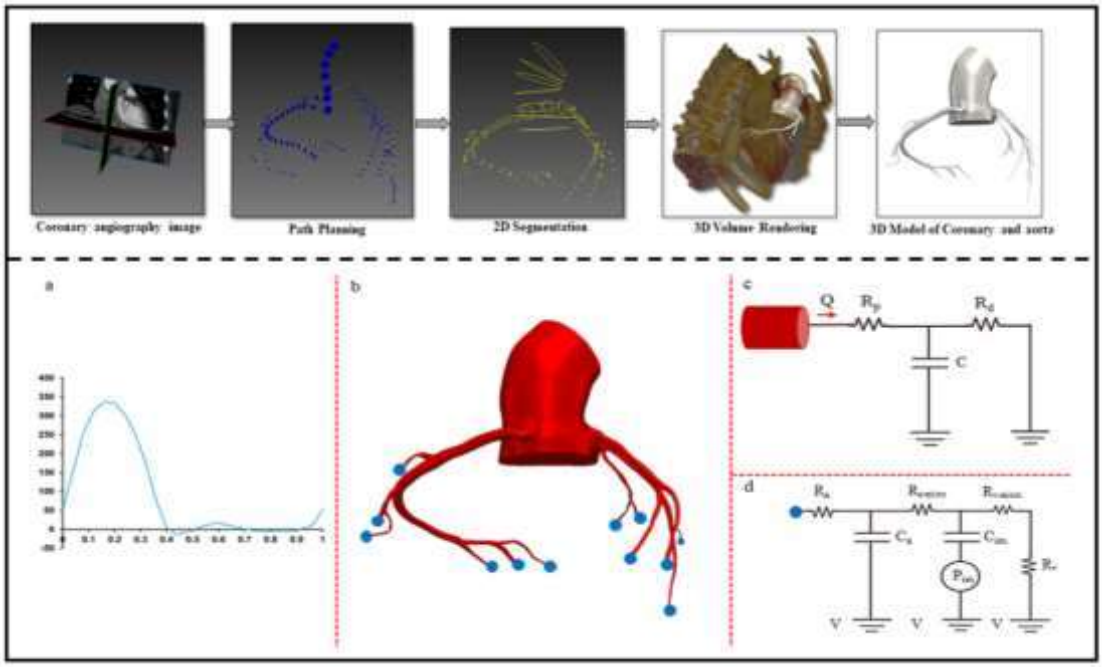

Sumit Kumar, B.V Rathish Kumar, S.K Rai. "Patient-Specific Blood Flow and Pressure Modelling of Suspected Coronary Artery Disease Using Open Loop System", AIP, Physics of fluids (IF 4.98), (Under review)

Chapter 5

Patient-Specific Blood Flow and Pressure Modelling of Suspected Coronary Artery Disease Using Open Loop System

5.1 Introduction

Coronary Artery Disease (CAD) is the most frequent cardiovascular disease (CVD), the primary cause of death today. CAD involves myocardial ischemia due to atherosclerotic build-up, which narrows the arterial lumen. Early prognosis and diagnosis of CAD could reduce this high morbidity rate and thus decrease the mortality rate. Coronary arteries receive blood straight from the left ventricle's ejection into the aorta and then feed blood to the myocardium. As a result, they have a high flow rate and pressure. Coronary arteries have complicated shapes, with numerous branches and being very curved. As a result, high pressure and flow rate into curved and branching coronary arteries disrupt flow patterns. Consequently, the endothelium of the arteries suffers from significant wall shear stress (WSS) leading atherosclerotic lesions, plaque development, and stenosis. Therefore, it is crucial to look at how complex shapes affect various hemodynamics parameters in a patient-specific coronary computed tomography angiography (CCTA) model. For computing cardiovascular hemodynamic some assessment tool has been developed. These cardiovascular assessment tools provide awareness to physicians to assist CVD diagnosis by allowing them to acknowledge indicators that lead to CVD. However, a more robust and holistic way is

the disclosure of the latest cardiac therapeutics and diagnostics of the heart. This has brought about the demanding domain of virtual design, simulation, and testing tools and technologies in a patient-specific and region-specific environment. The emergence of patient-specific computational fluid dynamics (CFD) has fore shadowed the latest domain of computer assisting diagnostics (Pinho et al., 2019b; Student et al., n.d.; Wu et al., 2015). The simulations of the cardiovascular blood flow offer a potential, non-invasive means to supplement the learnings from medical imaging and clinical measurements to influence clinical decision-making positively.

Computerized tomographic (CT) angiography is a valuable tool for evaluating not only coronary artery stenosis (Hamon et al., 2007; Motoyama et al., 2008) but also plaque properties (Cordeiro and Lima, 2006; Motoyama et al., 2007). Coronary computed tomography angiography (CCTA) noninvasively examines the coronary lumens for the identification of stenotic lesions. Patients with questionable CVD identify coronary lumen plaque and shapes property during initial visits (Helfant et al., 1970; Motoyama et al., 2009; Saremi and Achenbach, 2015). The Coronary Artery Disease Reporting and Data System (CAD-RADS), related to the finest-grade stenosis recorded by CCTA, came up with recommendations for supplementary supervision of patients with suspected CVD (Cury et al., 2016). Currently, to evaluate the operational intensity of moderate coronary stenosis (CAD-RADS $\geq$ 3), the fractional flow reserve (FFR) is extensively used, with the target of verifying the impact of the stricture (stenosis) on the myocardial ischemia (Hulten et al., 2013). In CAD patients, hemodynamic plays a vital role in the progression, evaluation, and treatment of cardiovascular disease. For personalized treatment planning, suitable quantities like shear stress of wall,

deformation of the vessel wall, blood pressure, streamlines, and velocity are used to explore the impact of mechanical stimuli in CVD (Davies et al., 2013; Morbiducci et al., 2016). Computational simulations have been demonstrated helpful in examining the hemodynamic of the cardiovascular system (Taylor and Figueroa, 2009). Assessing atherosclerosis and cardiac ischemia requires precise blood flow measurements due to stenosed arteries(Kang et al., 2018) . This includes: assessing hemodynamic of blood vessels of the healthy and diseased individuals, planning vascular surgeries, helping in the design and assessment of vascular medical devices (Li and Kleinstreuer, 2005), and the prognosis of the results of interventions (Migliavacca et al., 2006). Thus, the application of CFD analysis related to the patient-specific CCTAs in the domain of CVD has grown in recent years (Kumar et al., 2023, 2022; Taylor et al., 2013; Zarins et al., 2013).

Computational simulations have been seldom used to forecast pulsatile flow and pressure areas of three-dimensional CCTA, in part since the flow rate and pressure in the coronary vascular beds are highly related to the interactions between the heart and the arterial system. Unlike flow in other parts of the arterial system, coronary flow decreases when the ventricles contract and increase the intramyocardial pressure, which exerts an extravascular compressive force on the coronary vessels. In patients with coronary artery disease (CAD), local stenosis produces extreme hemodynamic and mechanobiological conditions that can precipitate occlusive thrombosis (Cao et al., 2021). Specifically, oscillatory low shear stress localizes endothelial dysfunction and atherosclerosis (Buradi and Mahalingam, 2020). Therefore, a patient-specific coronary modeling strategy should be considered in hemodynamics analysis. For simulating

coronary blood flow, three-dimensional (3D) image-based modelling and computational fluid dynamics are well-validated. However, 3D flow simulations of the entire coronary tree are computationally intensive. Consequently, they could become an impediment when contemplating cases with a vast array of scales or problems that evolve over time. Reduced-order models (0D) alone or in conjunction with higher-dimensional models provide a computationally feasible substitute to comprehensive three-dimensional (3D) patient-specific blood flow modelling. Recent studies have demonstrated the ability of reduced-order models to obtain coronary hemodynamic data, including estimations of hemodynamic parameters, the gold standard for assessing the functional significance of stenosis in CAD patients (Wong et al., 2020). A coupled reduced order model technique can address the limitations mentioned above by providing substantially reduced computational cost while maintaining the accuracy of the localized hemodynamics in the region of interest, namely the stenosis (Alimohammadi et al., 2017). Standardized person-specific and region-specific reporting will be helpful to reduce the variability of CADs among practitioners for maximizing the clinical impact of coronary CTA. Therefore, it is important to know the hemodynamics characteristics of patients having chest pain in the initial visit.

In this work, the suggested modelling approach uses both a low-order and a high-order approach to solve patient-specific problems and give a way to pre-diagnose a patient with coronary artery disease in the critical phase during the first visit. In this work, a new geometric modelling, localized mesh, tuned boundary conditions method is used to model and simulate a person with possible heart disease so that the hemodynamics factors during the cardiac cycle can be studied. Also, the framework calculates dynamic

(i.e., pulsating), patient-specific, and highly resolved hemodynamic conditions at a lower computing cost. This makes it possible to model cardiac hemodynamics in a way that is computationally feasible.

The main goal of this work is to come up with a method for open loop (0D-3D) analysis of pulsatile hemodynamics in patient-specific CCTA data that could be used in the future for multi-scale patient-specific cardiac simulations. The important hemodynamics parameters such as Velocity, Streamlines, WSS, TAWSS, OSI and RRT were evaluated and discussed in results. This study will provide the medical practitioner with some theoretical support for diagnoses and treatments of CADs.

5.2. Material and Methods

5.2.1. Patient Information

In this study, a patient of age 51 yrs. having chest pain underwent coronary computed tomography angiography (CCTA) examination for diagnosis of coronary artery disease (CAD) at a 128 slice CT scan center, SSH, Institute of Medical Science BHU, Varanasi, India. The study was supervised in conformity with the principles of the declaration of medical ethics requirements. Plain and CECT of the heart was done with sections acquired in axial plane in 0.625 mm slice thickness from the level of the main pulmonary artery to the diaphragmatic surface of the heart. 3D volume rendering and multiplanar reconstruction are used for better anatomical evaluation, and also calcium scoring was done prior to this in the plain scan. The scanning details of the patient are described in Table 5.1.

Table 5.1. Basic information of the patients at the time of initial visit.

Information	Patient data
Cardiac output ($Q_{systemic}$)	4426.2 ml/min
Slice thickness	2.5
Protocol Name	5.49 cardiac 128 slice new
Pixel Spacing	0.488281\0.488281
Series Description	SmartScore - Gated 0.35sec

5.2.2. Image-based three-dimensional geometrical modelling

To generate a patient-specific anatomic model based on CT angiography image data, the geometry of coronary artery and aorta was first reconstructed using an open-source modelling tool, i.e., SimVascular. It has been investigated that wide studies have been carried out in the area of medical image segmentation (Kim et al., 2010; Sankaran et al., 2012; Updegrove et al., 2017) and to conduct 2D and 3D image segmentation using open-source SimVascular (Updegrove et al., 2017) which is a suitable platform for medical image based 3D modelling and simulations.

The following procedure was carried out for 3D modelling such as visualization, path planning along vessel centerlines, creating cohorts of 2D contours of the vessels' lumen at vertical cross-sections, lofting a surface from the 2D contours for respective coronary vessel and merging separate vessels to form a complete solid model. In this work, techniques used for modelling were similar to (Cao et al., 2021; Updegrove et al., 2017). The detailed description of the step by step procedure for cardiovascular modeling using image data are described in (Figure 5.1).

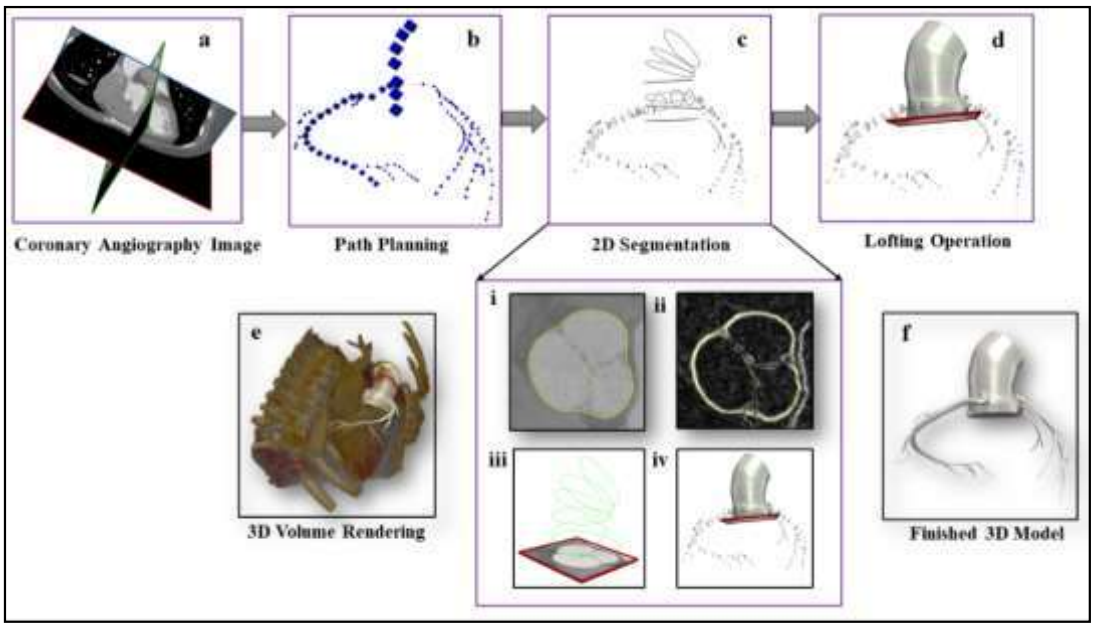

Figure 5.1 : Complete step by step process for cardiovascular modeling using image data, (a) image visualization, (b) Path planning (c) 2D Segmentation (i- image intensity, ii- contour of slice, iii- 2D contour ring generation & iv-lofting operation) (d) lofting operation (e) 3D volume rendering (f) Finished 3D model.

5.2.2.1 Path Planning:

The design of the pathways is an essential stage in establishing a method by which separate vessels may be connected to one another. In most cases, it is beneficial if the pathways overlap somewhat with one another. This will guarantee that the entrance of the branch vessel will fit completely inside of the main vessel. Additionally, it is preferable for the pathways to travel close to the center of the lumens of the vessel. This makes the segmentation aspect of the procedure much simpler. The first group is referred to as "Control Points," and the second group is called "Path Points." Control Points are used to define a vessel, and Path Points are computed using a spline that is based on the control points, as illustrated in (Fig. 5.2).

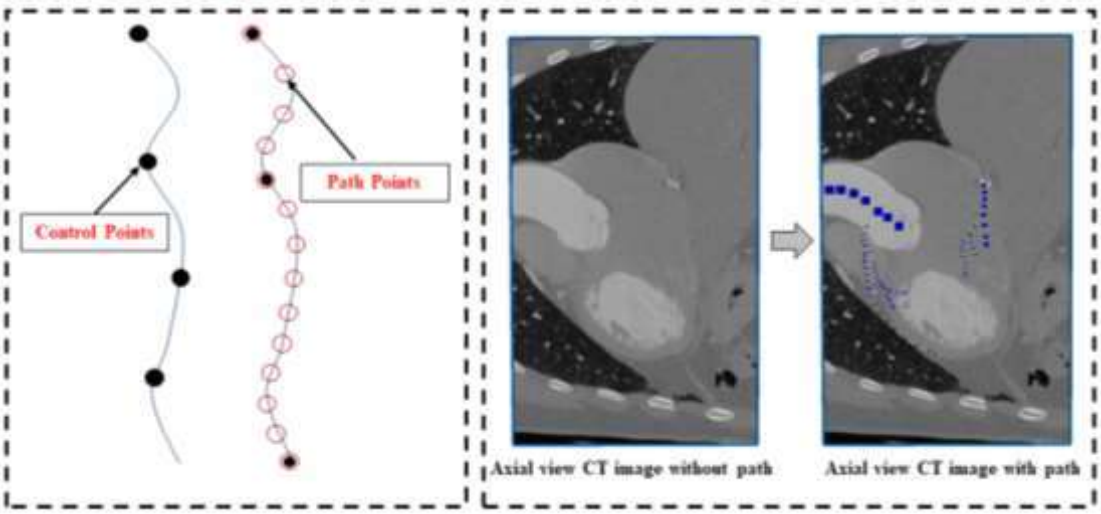

Figure 5.2 : Path planning of CT-coronary image of patient specific model

5.2.2.2 Segmentations:

Numerous studies have been conducted in the field of image segmentation, resulting in the creation of numerous techniques. These techniques seek to autonomously recognize objects and structures within an image. For our purposes, we desire to locate the vessel's lumen. In this modelling strategy, we only used 2D segmentation methods, which implies segmentations are conducted in a plane, as depicted in (Figure 5.3). To construct a 3D model from our 3D imaging data, we generate a series of 2D segmentations along a given path, which can then be merged together to form a 3D model. Limiting to define a Contour. The level set method is employed here for 2D vascular modelling. Using intensity image data and geometric constraints, these level sets generate a seamless contour of the vascular wall in 2D cross sections. Using the level set method, initialization with a sample is followed by two stages of segmentation. In stage1 parameters growth and end criteria are utilized to arrive at a solution approximation. Parameters such as Blur, Kthr, maximum iterations, and maximum error are used for this purpose. Based on the results of stage 1, the objective of stage 2

level set is to produce a seamless, accurate contour. In stage2, parameters such as Blue, Kupp, and Low are employed to specify the utmost allowable curvature. While sometimes it is not feasible to segment an image using automated techniques, segmentation is frequently possible. Occasionally, automatic techniques are effective but produce poor contours. In these instances, manual segmentation is preferable.

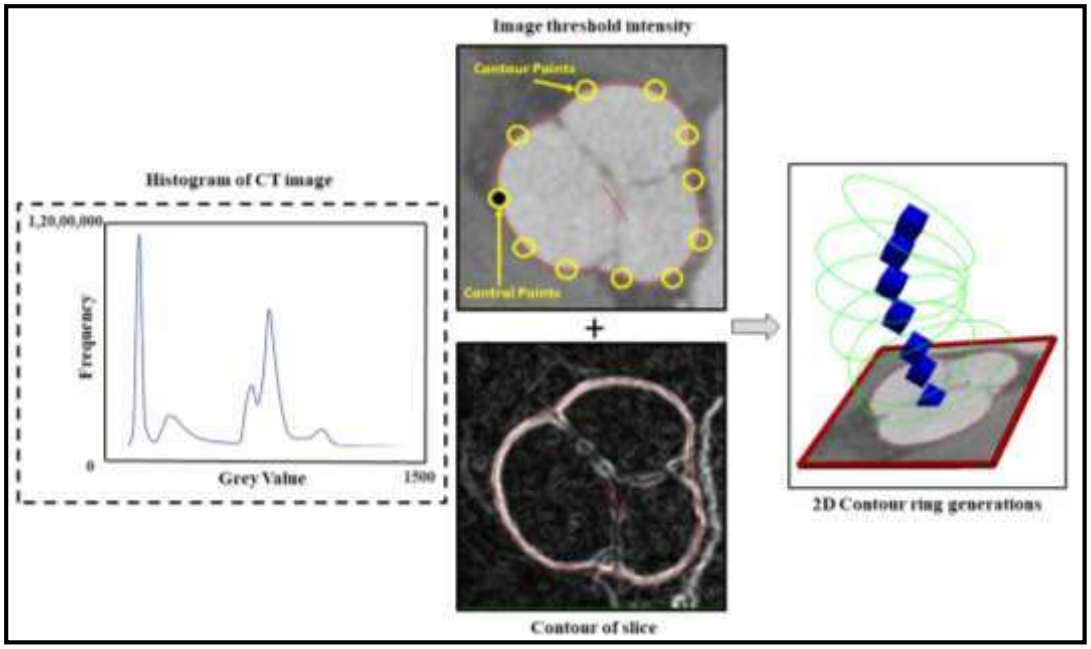

Figure 5.3 : 2D segmentation for coronary CT- angiography data

5.2.2.3.Lofting:

This is used to determine whether or not the contour group is of sufficient quality to be lofted into a 3D model in the future. This stage is really necessary in order to have a successful solid modelling experience later on. The step by step procedure in shown in (Figure 5.4).

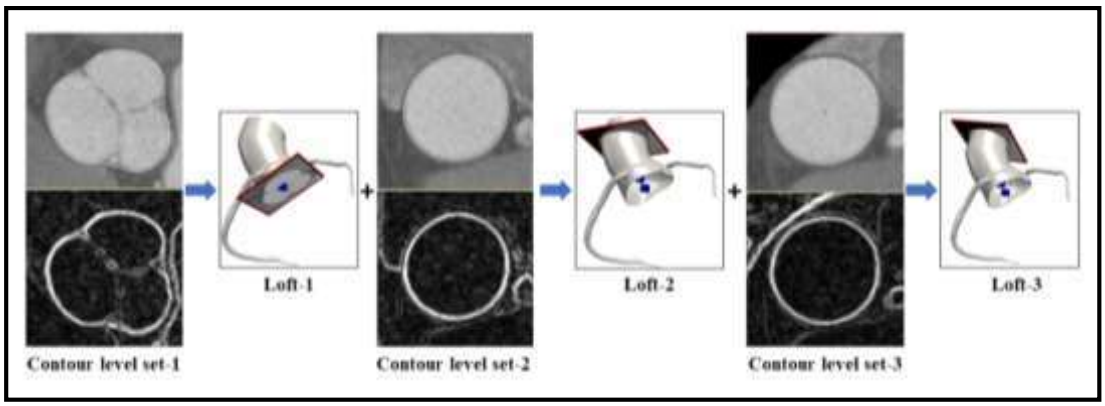

Figure 5.4 : Lofting operation after image segmentation

5.2.2.4 Solid modelling:

After lofting, solids are generated for each branch, resulting in an array of solid branches. The individual branches undergo union addition (Boolean addition). The result is a single solid region with defined boundaries that represents the blood flow domain. The aorta divides into two major branches, which provide blood to the heart (coronary arteries). The left main coronary artery (LMCA) and right main coronary artery (RMCA) are the common abbreviations for these two arteries. The left anterior descending artery (LAD) and left circumflex artery (LCX) are two offshoots of the left coronary artery. The left coronary artery supplies blood and oxygen to the heart's left chambers (the left ventricle and atrium), whereas the right coronary artery supplies blood and oxygen to the heart's right chambers (the right atrium and ventricle). It is common to see several tiny vessels that originate from these larger ones, particularly in high quality CT imaging data. The 3D anatomical models of coronary artery with notations is depicted in (Figure 5.5).

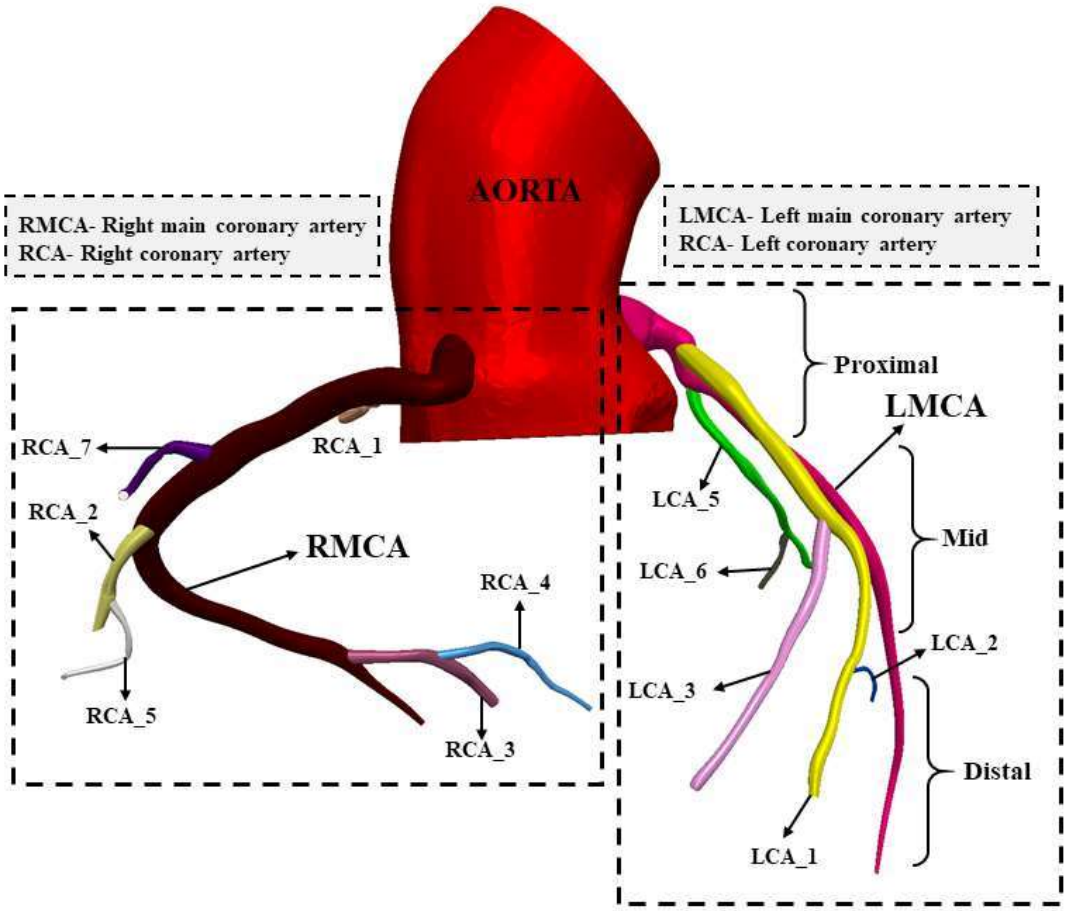

Figure 5.5 : Computational domain and anatomical notations of 3D coronary model for hemodynamics evaluation

5.2.3 Meshing

Once we have a solid model representing a region of interest, we need to discretize the flow domain into tiny pieces (called elements) for simulation. The tetrahedral meshing is preferred mainly in the case of biological complex models (Updegrove et al., 2017; Wong et al., 2009). Here in this case TetGen developed by Hang Si through WIAS in Berlin and the Vascular Modeling Tool Kit (VMTK) libraries is used. In accordance with the SimVascular guideline and the mesh independency test was performed, the global size of the finite volume mesh for the coronary arteries was set to 0.02 mm and

0.2 mm for the aorta. While in blood flow simulation, interesting phenomena can happen near the vessel walls, so it is beneficial to consider increased mesh density in the areas of high gradients. Four boundary layers were used with the portion of edge size 0.5 mm and layer decreasing ration 0.8. In resulting fine mesh details of the model are: elements 101609912, nodes 16379644, edges 2506143 and faces 1670762 with unstructured triangular elements. The walls of the models were assumed as rigid. Mesh visualization illustrated in (Figure 5.6) shows the meshing of aorta wall, inlet, outlet and coronaries arteries with boundary layer mesh. Also, the mesh details and grid independence are shown in Table II.

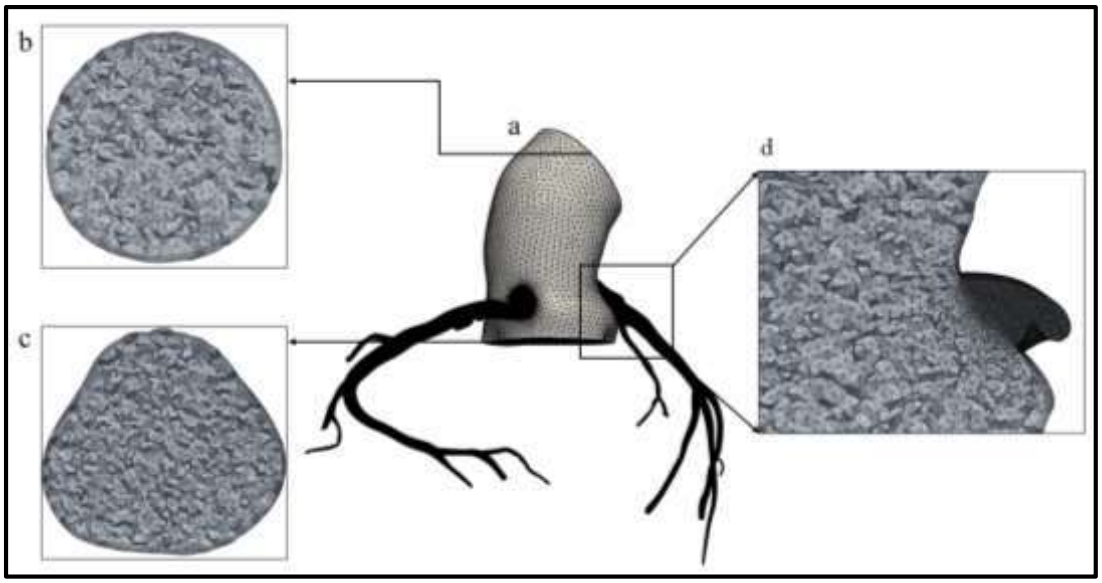

Figure 5.6 : Mesh visualization of the model (a) Main 3D model (b) & (c) Inlet and outlet with boundary layer mesh view (d) Coronaries arteries mesh view

In the domain of meshing, there are three fundamental challenges: robustness, mesh quality, and computational efficacy in mesh generation. For complex geometries, tetrahedral mesh elements are the finest option. In this problem, a tetrahedral shape maker based on a finite octree is used. The basic idea behind finite-octree methods is

to break up a complicated shape into smaller, easier pieces. Then, using a mesh generation technique (such as templates, the Delaunay triangulation) shown in (Figure 5.7), the individual pieces are connected. In order to enhance the quality of the provided finite element analysis, it was necessary in this problem to increase the mesh density locally in regions with complex behavior using spherical refinement. As shown in Table 5.2, the global mesh element size is set to 0.2 mm, and Mesh1, Mesh2, and Mesh3 are configured for local mesh size.

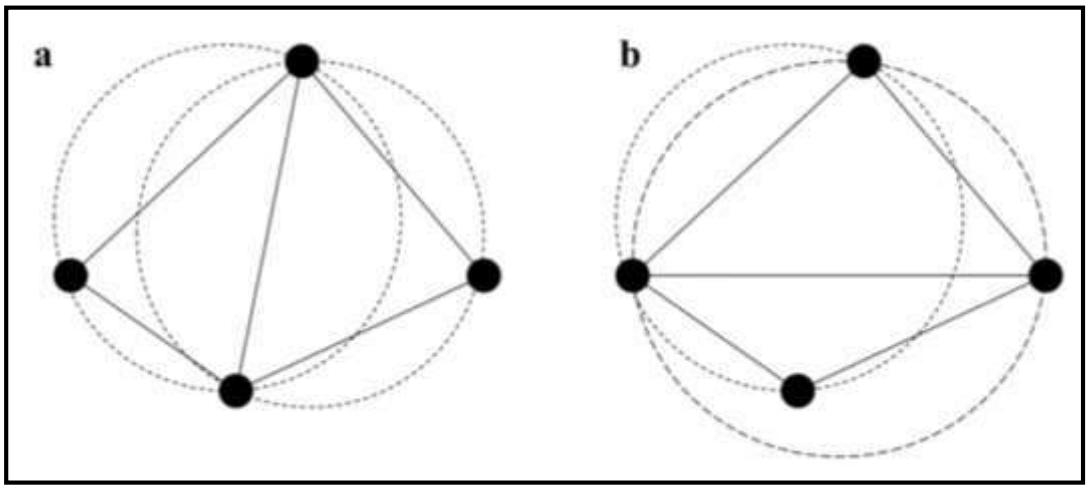

Figure 5.7 : Delaunay criterion. According to the Delaunay criterion, no other point in the triangulation can lie beneath the circumscribing sphere (circle in 2-D) of the points that define a simplex in the triangulation. Figure (a) illustrates a Delaunay triangulation of four locations in R2, whereas Figure (b) illustrates a non-Delaunay triangulation of the same four points.

Table 5.2. Mesh details of coronary model

Properties	Elements	Nodes	Edges	Faces
Mesh 1 (Global estimate size 0.001 and aorta 0.2 mm)	101609912	16379644	2506143	1670762
Mesh 2 (Global estimate size 0.002 and aorta 0.2 mm)	105877295	17248904	2516550	1677700
Mesh 3 (Global estimate size 0.003 and aorta 0.2 mm)	34139561	5638692	1108155	738770

5.2.4 Mesh Independency Test

To do mesh validation, fine (0.001mm), coarse (0.002 mm), and medium (0.003 mm) three type mesh size is considered and mesh visualization is shown in (Figure 5.6). Mesh validation was performed using plot of flow rate at cap_Aorta_2 with respect to the cardiac cycle of the coronary model is also described in (Figure 5.8).

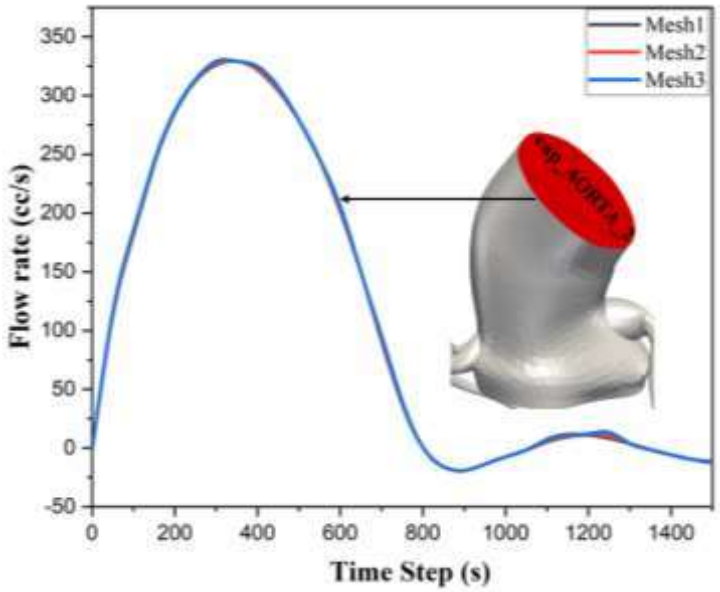

Figure 5.8 : Mesh independency check; depicting flowrate with respect to time step from cap_Aorta_2 of the model

5.2.5 Open Loop (0-3D) Finite Element Modelling

Here in this modelling approach compared to a complete 3D model of the coronary tree, the computing time of this (0D-3D) linked modeling technique is much lower, making it a good candidate for usage in conjunction with an LPN model that mimics the microscopic events of blood circulation toward a fully multiscale model. We had defined a Windkessel RCR boundary condition at the aortic outflow. The Windkessel model consists of three parts: a proximal resistance, representing the viscous resistance

of the arterial vasculature just downstream of the model; a capacitor, representing the vessel compliance of all downstream vasculature; and a distal resistance, representing the resistance of the capillaries and venous circulation. By adjusting these values, we can ensure that the simulated pressures are accurate representations of the actual physiologic states of the patient. We use a modified lumped parameter model to simulate the phase characteristics of coronary flow and pressure waveforms at the coronary outlets. The inclusion of the pressure source P_{im} is the primary innovation of this model. This is the pressure within of the heart. It is necessary to provide a flow waveform that simulates the flow out of the aortic valve for the inflow in the coronary simulations to be effective. The various hemodynamic parameters like Pressure Drop, Velocity Profile, WSS, TASSS, OSI, FFR and streamlines can be investigated using a three-dimensional (0D-3D) open-loop modelling approach of the coronary arteries from CCTA, which can be seen in (Figure 5.9).

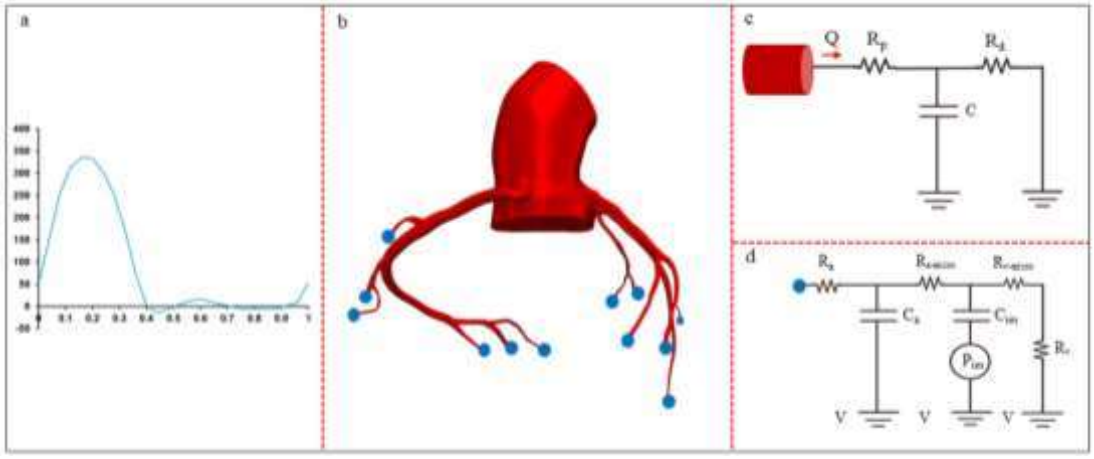

Figure 5.9 : Diagram of image-based 3D model of the patient-specific aorta and coronary arteries coupled to open-loop, inflow waveform, systemic and coronary circulations.(a) Inlet flowrate wave (b) 3D geometry of coronary model (c) Windkessel RCR boundary conditions (d) coupled to lumped parameter coronary vascular model.

5.2.6 Governing Equations & Simulation Setup

In the current study, blood was assumed to be incompressible, laminar, unsteady, homogenous, and Newtonian. For solving blood flow in the SVsolver, blood density was (1.06 g/mL) and dynamic viscosity of (0.04 dyne. s/cm^2) for all simulations. Blood vessel walls were assumed to be rigid in all cases. A time-step size of 0.001 ms was chosen to satisfy the stability condition. Simulations were run for 6 cardiac cycles until the pressure fields at the inlet and outlet did not change more than 1% from the previous cycle. A workstation of 48 cores processor with 64 GB RAM and an 8 GB graphics card was used to carry out the CFD simulations. The simulations performed in order to evaluate the hemodynamics parameters like velocity distribution, flow patterns, wall shear stress, oscillatory shear index, and vorticity in the localized region of interest coronary models. Blood flow was modelled using the incompressible Navier–Stokes equations NSEs and the corresponding governing equations for NSEs were:

$$\rho\vec{v},t + \rho\vec{v}.\nabla\vec{v} = -\nabla p + div(\tau) + \vec{f}\ ,\ (\vec{x},t) \in \Omega \times (0,T) \ldots\ldots\ldots (1)$$

$$div(\vec{v}) = 0\ for\ (\vec{x},t) \in \Omega \times (0,T) \ldots\ldots\ldots (2)$$

$$\text{Where}\quad \tau = \mu(\nabla\vec{v} + (\nabla\vec{v})^T) \ldots\ldots\ldots (3)$$

$$u = g,\quad x \in \Gamma^g \ldots\ldots.(4)\ \text{(Dirichlet BC)}$$

$$T.n = h,\ x \in \Gamma^{gh} \ldots\ldots(5)\ \text{(Neumann BC)}$$

Where Γ is the boundary of fluid, which is divided into a Dirichlet boundary region Γ^g and a Neumann boundary region Γ^h, $\vec{v}$ is the velocities, p is the pressure and ρ is the density.

5.2.7 Hemodynamic Parameters

To assess the wall shear stress acting on the lumen wall under pulsating flow in human heart circulation, Time Average Wall Shear Stress (TAWSS), Oscillatory Shear Index (OSI) and of Relative Residence Time (RRT) can be used. From previous work, it was observed that abnormal TAWSS (< 4dyne/cm^2 or 40 dyne/cm^2) might cause blood platelet activation, cell aggregation, platelet activation, and inflammatory cell-mediated destructive remodeling (Xiang et al., 2014). TAWSS is defined as:

$$TAWSS = \frac{1}{T} \int_0^T |WSS|\, dt \quad \text{.....(6)}$$

Where T is the period of the cardiac cycle, and WSS is the WSS vector.

To evaluate axial directional change in WSS within the cardiac cycle Oscillatory Shear Index (OSI) are a frequently used index. Also, abnormal OSI shows that the flow field is highly disturbed, associated with the formation of thrombosis (Xiang et al., 2014). OSI is defined as follows:

$$OSI = 0.5 \times \left[1 - \frac{\left|\int_0^T WSS dt\right|}{\int_0^T |WSS| dt}\right] \text{..... (7)}$$

Where T is the period of the cardiac cycle, and WSS is the WSS vector.

$$RRT = \frac{1}{TAWSS \times (1 - 2 \times OSI)} \quad \text{..... (8)}$$

5.2.8 Boundary Conditions

All the blood flow dynamic parameters in the simulation were analyzed using SimVascualr (I.E vignon-clementel, 2018). In this modelling approach we have two

type of boundary conditions namely boundary condition at the aorta and at the coronary arteries. For inlet pulsatile velocity, a normal human flow waveform is shown in (Figure 5.9 (a))was considered. For modelling the physiology of coronary circulation and microcirculation, the boundary conditions downstream of the coronary artery are critical. Coronary boundary conditions were applied at each coronary outlet of the model, standard RCR (Windkessel) boundary conditions (Vignon-Clementel et al., 2006), the outlets of the aorta and bifurcated vessels. The below equations were used for patient-specific parametric modelling and shown in Table 5.3.

The flow transportation to each major component of the coronary arteries was determined using morphology data and hospital data. Murray's law was first put forward in 1926 (Murray, 1926), and it defines the physical principles for fluid flow across branching transfer networks that are present in a broad variety of biological systems. In human arteries, Murray's law describes the ideal balance that should exist between the forces exerted by friction and those exerted by metabolic processes. Therefore, the amount of energy needed to push blood through the coronary circulation (overcoming vascular resistance) is counterbalanced by the amount of energy needed to create and maintain the blood volume in such a way that the total amount of energy needed is reduced. This allows for the overall energy expenses to be reduced. Murray's law, on the other hand, assumes that a Newtonian fluid moves in a steady, laminar flow through rigid tubes of constant volume. On the other hand, blood flow in the coronary arteries of humans is pulsatile and may be disrupted when atherosclerotic stenoses are present. across addition, a variety of studies that are based on archetypal geometries across a broad range of realistic networks (Bejan et al., 2000; Miguel, 2019; Revellin

et al., 2009; Soni et al., 2020) when applied to Newtonian and non-Newtonian fluids, generally recover the fundamental form of Murray's law with varied exponent values. We postulated that the average coronary flow represents 4% of cardiac output (Opie, 2004). On the basis of mean flow and designated venous pressure, coronary venous resistance was calculated for each coronary outlet surface based on literature data (Opie,2004). Usisng literature data, we calculated coronary arterial and microcirculation resistance based on mean flow, mean arterial pressure, and the coronary impedance spectrum. Using published data (Van Huis et al., 1987) the capacitance values were modified to generate coronary flow and pressure waveforms that were physiologically realistic. Literature-based modifications were made to the coronary parameter values for each coronary outlet surface by reducing the total resistances and raising the capacitances and the ratio of the coronary arterial resistance to the total coronary resistance. The parameter values of three-element Windkessel models have been established to match subject-related cardiac output and pulse pressure. Table.5.3 outlines the specifics of adjusting patient data and calculations. The final parameter values of all boundary conditions at outlet are shown in Table 5.5.

Table 5.3. Equation for patient-specific parametric modelling

$Q_{c,t} = 0.04\ Q_{St} = 2.9508\ ml/s$	$R_{c,t} = 25\ R_{s,t}$
$R_{s,t} = \frac{P_{mean}}{Q_{s,t}} = \frac{100\ mm/Hg}{73.77\ ml/sec} = 1.355\ mm\ Hg/ml$ …… (9)	
$\frac{Q_{lc}}{Q_{rc}} = \frac{7}{3} = \gamma$, $R_{lc,t} = R_{c,t} . \frac{(1+\gamma)}{\gamma}$ …..(10)	$Q_{branch} \sim d^m$, m=3
$Q_{branch} \sim d^m$, $R_{branch} \sim d^{-m}$,	$R_{branch} \sim \sqrt{A}$

$R_{c,i} = R_{c,t} \frac{\sum_j^N (\sqrt{A_j})^{2.6}}{(\sqrt{A_j})^{2.6}}$ .....(11) $R_{a,i} = 0.32 * R_{c,i}$ .....(12)	$R_{a,m} = 0.52 * R_{c,i}$ ..... (13) $R_v = 0.16 * R_{c,i}$ ..... (14)
Murray's Law (Zhou et al., 1999) **m** (**murray's index**) = 2.6 $C_{lc,t} = 3.6 * 10^{-5}$ $cm^5/$ dyne , $C_{rc,t} = 2.5 * 10^{-5}$ $cm^5/$ dyne, $C_{branch} \sim A$ .....(15)	
$R_{c,i} = R_{c,t} \frac{A_j}{\sum_j^N A_j}$, $C_a = 0.11 * C_{c,i}$, $C_{im} = 0.89 * C_{c,i}$ .....(16)	
$R_d + R_p = \frac{P_{mean}}{Q_{aorta}}$ R_{cor}: R_{aorta} = Q_{aorta}: Q_{cor} .....(17)	

where R_p was the viscous resistance of the downstream arterial vasculature, R_d was the resistance of the capillaries and venous circulation, P_{mean} was the mean pressure, R_{cor} and Q_{cor} represented the total resistance and the cardiac output of coronary arteries (mL/s) and R_{aorta} and Q_{aorta} represented the total resistance and the cardiac output of the aorta. The resistances for each coronary outlet could be split into R_a (arterial resistance), $R_{a-micro}$ (microcirculation resistance), R_v (venous resistance), C_a (microcirculation compliance), C_{im} (myocardial compliance), and P_{im} (intra-myocardial pressure).

5.2.9 Inlet Boundary Condition

A characteristic aortic pulse form was applied at the inlet of the aorta Fig 5.9 (a) as a Dirichlet boundary condition. The flow of the pulse waveform was scaled to match the patient-specific cardiac output and the heart rate of the patient received from echocardiographic and clinical data.

5.2.10 Coronary Boundary Conditions

By combining together, the pressure in the aorta and the resistance in the coronaries further downstream, blood flow at the intake to the coronaries can potentially be guaranteed. On the other hand, during systole, the distal coronary resistance dramatically increases as a result of the growing intra-myocardial pressure that results from the contraction of the heart. The flow of blood via the aorta and the pressures inside the ventricles both have an effect on the pressure inside the myocardium. Therefore, there is a delicate synergy between the flow at the coronary outputs and the aortic flow at the intake, and this is something that the numerical model has to be able to capture accurately.

An open-circuit resemblance lumped parameter network (LPN) were constructed to model coronary flow and pressure depicted in (Fig. 5.9). followed by earlier work (Kim et al., 2010)·(Cao et al., 2021). The model is composed of resistors that model the influence of viscosity and downstream pressure, capacitors that model the vessel acquiescence, and a time-varying pressure to model the contracting ventricle. This model is ruled by ordinary differential equations with a known analytic solution, as described below in the equations. The equation was implicitly coupled with the coronary outlet boundaries in the finite element solver.

The seven parameters of the LPN coronary model must be tuned to match clinical and literature data. These are arterial resistance (R_a), microcirculation compliance (C_a), microcirculation resistance ($R_{a-micro}$), venous microcirculation resistance ($R_{v-micro}$),

myocardial compliance (C_{im}), venous resistance (R_v), and intra-myocardial pressure ($P_{im}(t)$). In this model, all the resistances are in series. As described in the next section, the intramyocardial pressure is determined from the ventricular pressures obtained from a lumped parameter heart model.

Our approach to determining parameter values are shown in the following paragraphs. The total coronary flow was considered to be 4% of the entire cardiac output of the patient (Bogren et al., 1989; Kim et al., 2010) and the flow percentages to the right and left coronaries were taken to be 40 and 60% of the total coronary flow (Johnson et al., 2008) respectively. The flow separation to individual coronary outlet branches in the LCA and RCA was weighted according to the outlet areas of the cap. The total resistance ($R_a + R_{a-micro} + R_{v-micro} + R_v$) at a specific coronary outlet was initially determined by the ratio of the mean pressure to the mean flow through that vessel, where the average blood pressure is determined by (SBP + 2*DBP)/3. SBP and DBP are the systolic and diastolic blood pressure, sequentially, as measured in the clinic. The corresponding values of resistances (R_a, $R_{a-micro}$, $R_{v-micro}$ and R_v) and capacitances (C_a and C_{im}) were calculated in accordance with the patient morphological data as similar to (Burattini et al., 1985; Kim et al., 2010). The total resistance and capacitance values for the RCA and LCA were then tuned over many flow simulations such that the total coronary flow matched the target values, and the peak systolic to diastolic flow ratio evened typical values for healthy patients (Kuijer et al., 2001).

The coupling of pressure P(t) with the flow rate Q(t) at the coronary outlet boundaries in the finite element solver was done through the following equation using the coupled

multi-domain method of as (Vignon-Clementel et al., 2010) implemented in the work of (Kim et al., 2010).

$M = \left[M_{\sim m}, \vec{M}_c\right]_{\Gamma_{hcork}}$ it defines boundary operator and

$H = \left[H_{\sim m}, \vec{H}_c\right]_{\Gamma_{hcork}}$ represent the traction and flow at each coronary outlet surface Γ_{hcor_k}

$$[M_{\sim m}\,(\vec{v}, p) + H_{\sim m}]_{\Gamma_{hcor_k}}$$

$$= -\left(R\int_{\Gamma_{hcork}} \vec{v}(t).\vec{n}d\Gamma + \int_0^t e^{\lambda_1(t-s)} Z_1 \int_{\Gamma_{hcork}} \vec{v}(s).\vec{n}d\Gamma ds\right) I_{\sim}$$

$$+\left(\int_0^t e^{\lambda_2(t-s)} Z_2 \int_{\Gamma_{hcork}} \vec{v}(s).\vec{n}d\Gamma ds - \vec{n}\cdot\tau\cdot\vec{n}/_{\Gamma_{hcork}}\right) + \tau_{\sim}/_{\Gamma_{hcork}} -$$

$$\left(Ae^{\lambda_1 t} - Be^{\lambda_2 t}\right) I_{\sim} - \left(\int_0^t e^{\lambda_1(t-s)} Y_1\, P_{im}(s)ds - \int_0^t e^{\lambda_2(t-s)} Y_2\, P_{im(s)ds}\right) I_{\sim}$$

……..(18)

$$\left[\vec{M}_c(\vec{v}, p) + \vec{H}_c\right]_{\Gamma_{hcor_k}} = \vec{v}/_{\Gamma_{hcor_k}} \quad \text{…….(19)}$$

P(t) and Q(t) are pressure and flow at the coronary outlet

$I_{\sim}$ is the identity tensor

The coefficient $\lambda_1, \lambda_2, A, B, R, Z_1, Y_1, Z_2, Y_2$ are defined using lumped parameter model of down -

stream coronary vascular bed as follow

$$\lambda_1 = \frac{-p_1 + \sqrt{{p_1}^2 - 4p_0p_2}}{2p_2}$$

$$\lambda_2 = \frac{-p_1 - \sqrt{{p_1}^2 - 4p_0p_2}}{2p_2}$$

$$A = \frac{-1}{\sqrt{{p_1}^2 - 4p_0p_2}}\left[(q_2\lambda_1 + q_1)Q(0) + q_2\frac{dQ}{dt}(0) + b_1p_{im}(0) + p_2\left(\lambda_2 p(0) - \frac{dP}{dt}(0)\right)\right]$$

$$B = \frac{-1}{\sqrt{{p_1}^2 - 4p_0p_2}}\left[(q_2\lambda_2 + q_1)Q(0) + q_2\frac{dQ}{dt}(0) + b_1p_{im}(0) + p_2\left(\lambda_1 p(0) - \frac{dP}{dt}(0)\right)\right]$$

$$R = \frac{q_2}{p_2}$$

$$Z_1 = \frac{q_2\lambda_1^2 + q_1\lambda_{1+}q_0}{\sqrt{{p_1}^2 - 4p_0p_2}}$$

$$Y_1 = \frac{b_1\lambda_1 + b_0}{\sqrt{{p_1}^2 - 4p_0p_2}}$$

$$Z_2 = \frac{q_2\lambda_2^2 + q_1\lambda_{2+}q_0}{\sqrt{{p_1}^2 - 4p_0p_2}}$$

$$Y_2 = \frac{b_1\lambda_2 + b_0}{\sqrt{{p_1}^2 - 4p_0p_2}}$$

With the following coefficients:

$$p_0 = 1$$

$$p_1 = R_{a-micro}C_a + (R_v + R_{v-micro})(C_a + C_{im})$$

$$p_2 = C_a C_{im} R_{a-micro}(R_v + R_{v-micro})$$

$$q_0 = R_a + R_{a-micro} + R_v + R_{v-micro}$$

$$q_1 = R_a C_a(R_{a-micro} + R_v + R_{v-micro}) + C_{im}(R_a + R_{a-micro})(R_v + R_{v-micro})$$

$$q_2 = C_a C_{im} R_a R_{a-micro}(R_v + R_{v-micro})$$

$$b_0 = 0$$

$$b_1 = C_{im}(R_v + R_{v-micro})$$

Using these operators, we couple the flow and pressure at each coronary outlet surface between the upstream three-dimensional finite element model and the downstream lumped parameter model.

5.2.11 RCR Boundary Conditions

RCR boundary conditions were applied at all other outlets to model the remaining downstream vasculature. The total resistance of all the outlets was calculated as the ratio of mean pressure to mean flow. The total capacitance values were adjusted to match the measured blood pressure of the patient. The details of patient-specific boundary conditions of various hemodynamic parameters are described below in Table (5.4 and 5.5).

Table 5.4. Parameter values of the coronary's outlets using coronary boundary conditions

Parameters	Conditions	Values
R_p	RCR	141.01
R_d	RCR	1416
C	RCR	0.001

Table 5.5. Calculated coronary boundary conditions parameters (R_p, C_a $R_{a\text{-}mic}$, C_{min} and R_v)

Name	Boundary Condition's type	Boundary conditions parameters values				
		R_p	Ca	Ra-mic	C_{im}	Rv
CAP_LCA1	Coronary	149833.2215	1.0621e-06	77913.27518	8.5934e-06	74916.61075
CAP_LCA2	Coronary	1600838.891	1.7172e-07	832436.2233	1.3894e-06	800419.4455
CAP_LCA3	Coronary	163938.219	9.9108e-07	85247.87389	8.0188e-06	81969.10951
CAP_LCA5	Coronary	223123.3905	7.8187e-07	116024.1631	6.3261e-06	111561.6953
CAP_LCA6	Coronary	252754.2522	7.1036e-07	131432.2111	5.7475e-06	126377.1261
CAP_LMCA	Coronary	1020172.602	2.4285e-07	530489.7528	1.9649e-06	510086.3008
CAP_RC3	Coronary	45546.71417	7.3266e-07	23684.29137	5.9279e-06	22773.35709
CAP_RC4	Coronary	326118.4176	1.6117e-07	169581.5771	1.3040e-06	163059.2088
CAP_RC5	Coronary	364690.8137	1.4789e-07	189639.2231	1.1965e-06	182345.4068
CAP_RC7	Coronary	125139.8861	3.3671e-07	65072.74079	2.7243e-06	62569.94306
CAP_RCA	Coronary	302481.3572	1.7077e-07	157290.3058	1.3817e-06	151240.6786
CAP_RCA1	Coronary	64632.93024	5.5974e-07	33609.12372	4.5288e-06	32316.46512
CAP_RCA2	Coronary	54182.18665	6.4107e-07	28174.73706	5.1868e-06	27091.09333

5.3 Results

The study results focus on important factors flow rate, streamlines, WSS, TAWSS, RRT, and OSI. All the simulations were performed for 6 cardiac cycle and the results are plotted for one cardiac cycle.

5.3.1 Flow rate and pressure distribution

5.3.1.1 On the outlet of the cap RCA

Flow rate and pressure waveforms of the right coronary artery (RCA) outlet caps in the coronary model are shown in Figure 5. 10 (a) & (b). It is noted from flow rate output from all caps of right coronary artery that the maximum flow rate ranges 0 < flowrate ($\dot{Q}$) <1.4 cc/s. Also, flow rate waveforms were high in systolic phase and low in the

diastolic phase. Thus, the adoption of the boundary conditions successfully captured the physiologic behavior of coronary flow. From Figure 5.3.1.1 (b) which depicts the pressure waveforms of the RCA it is noted that the pressure across the RCA outlet caps are in the range 0< Pressure< 80 mmHg. During systole, the pressure within the myocardium is high, which reduces the amount of blood that can flow through the coronary arteries. On the other hand, the pressure inside the myocardium is low during diastole, which allows for a greater amount of blood to flow.

5.3.1.2 On the outlet of the cap LCA

Figure 5.11 (a) & (b) depicts the flowrate and pressure waveforms of the left coronary artery (LCA) outlet caps in the coronary model. It is noted from flow rate output from all caps of LCA that the maximum flow rate ranges 0 < flowrate ($\dot{Q}$) <0.8 cc/s. From Figure 5.11 (b) which depicts the pressure waveforms of the LCA it is noted that the pressure across the LCA outlet caps are in the range 0< Pressure< 80 mmHg which is similar to RCA.

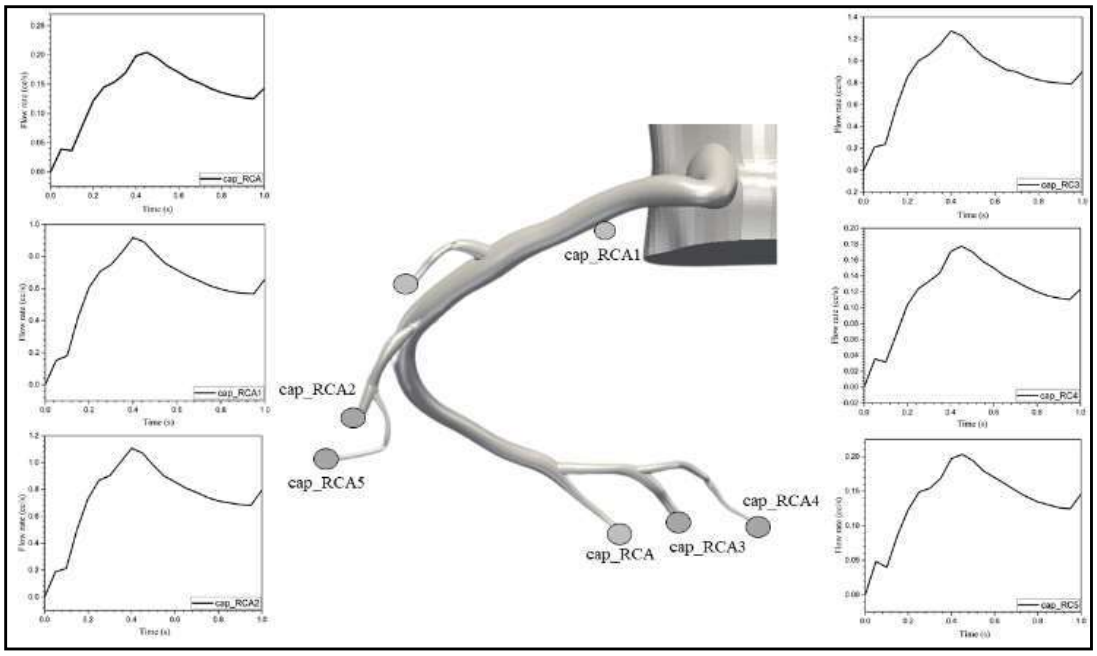

(a)

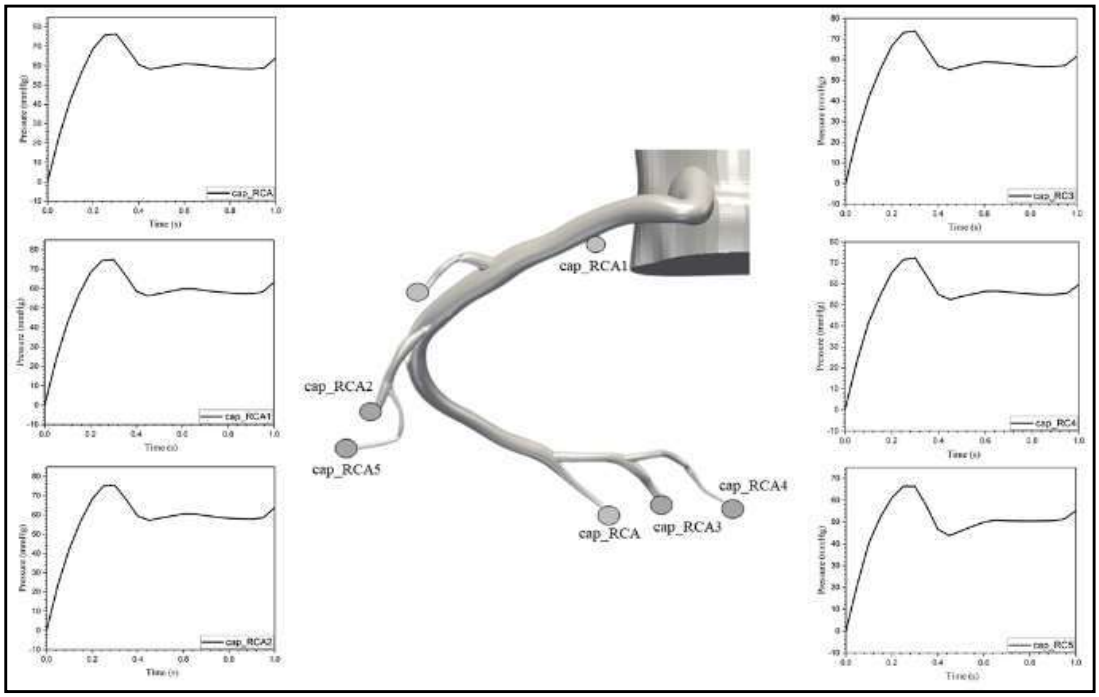

(b)

Figure 5.10 : (a) Flow rate and (b) Pressure waveforms of right coronary arteries at outlets (cap_RCA, cap_RCA1, cap_RCA2, cap_RCA3, cap_RCA5, cap_RCA5) during one cardiac cycle.

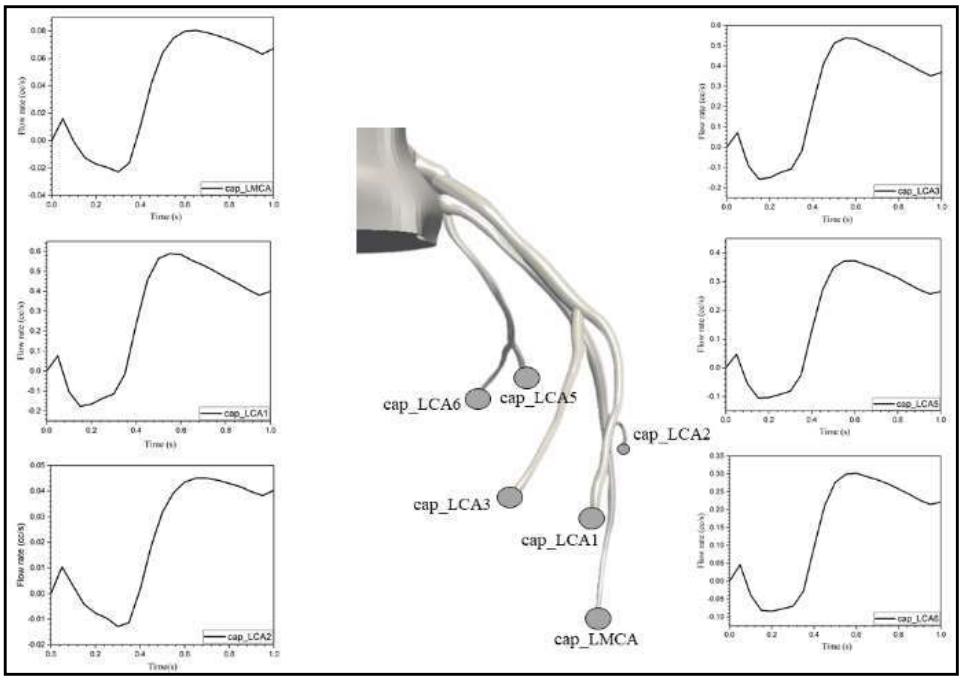

(a)

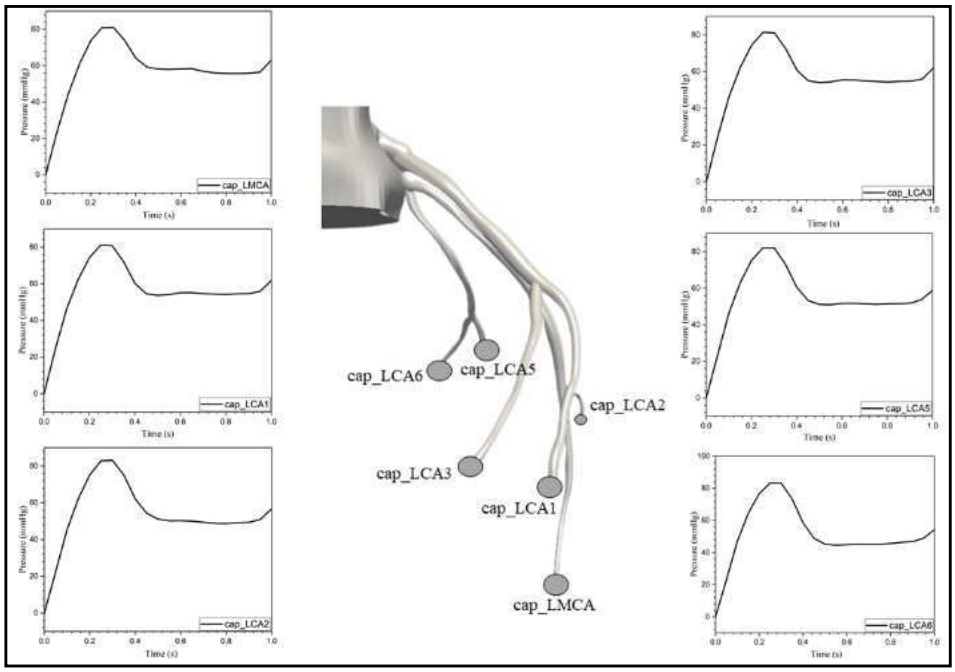

(b)

Figure 5.11 : (a) Flow rate and (b) Pressure waveforms of left coronary arteries at outlets (cap_LMCA, cap_LCA1, cap_LCA2, cap_LCA3, cap_RCA5, cap_RCA6) during one cardiac cycle.

5.3.2 Streamline visualization in the RCA during cardiac cycle

To visualize the flow lines in the coronary circulation, here right side of the coronary artery is selected during (T_1-T_6) instant of cardiac cycle as shown in (Figure 5.12). It is observed from the flow lines that from start of systole to peak of systole i.e. T_1-T_3, irregular flow lines are present, however during diastolic phase the flow lines shows regular pattern and with full streamlines length. There was no visible blood flow disorder, with low velocity in the proximal and middle LAD during the whole cardiac cycle. This was despite the fact that there was no obvious blood flow abnormality.

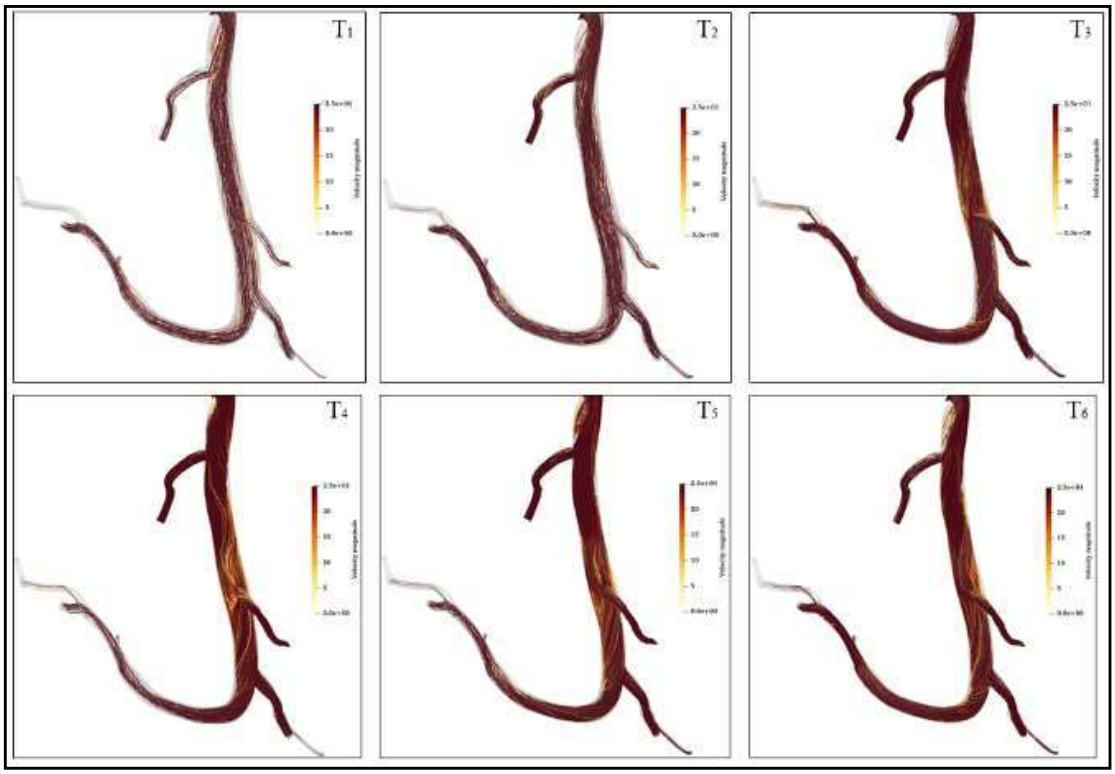

Figure 5.12 : Streamlines of blood flow in the (RCA) at T_1, T_2, T_3, T_4, T_5 and T_6 instant of cardiac cycle

5.3.3 Wall shear stress (WSS) contour during cardiac cycle

By definition, the WSS is the shear stress experienced by the vessel wall during the flow of blood, as given by:

$$WSS(\tau_\omega) = -\mu \frac{\partial u_t}{\partial n} |_{wall} \text{ .....(18)}$$

where μ is the dynamic viscosity, u_t is the wall tangential velocity, n is the unit vector that is vertical to the vessel wall. Wall shear stress contour distribution during important instant of cardiac cycle i.e. from T_1 to T_8 are depicted in (Figure 5.13 (a), (b)). To see in detail visualization of stress magnitude on the wall surface, both views of the model (anterior and posterior view) have been considered. From (Figure 5.13. (a)) it has been noted that from start of systole to end of systole (T_1-T_4) that WSS magnitude is maximum in the RMCA, LCA_1 and LCA_2 wall of the coronary model. Also, the maximum magnitude of WSS i.e. 75 Pa are marked with blacked circle. It is observed from (Figure 5.13) (a) & (b) that right coronary arteries experience higher wall shear stress fields in late systole late diastole whereas the left coronary arteries experience lower wall shear stress fields in the bifurcated arteries of LMCA.

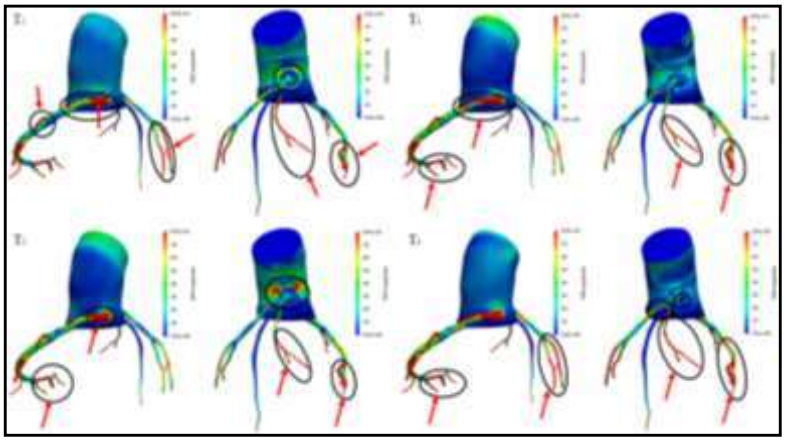

(a) (T_1-T_4)

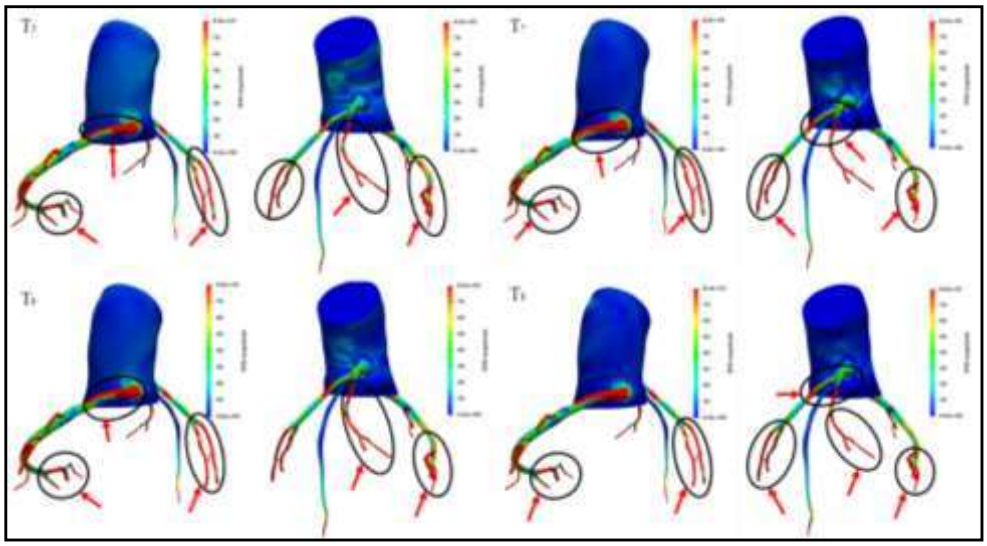

(b) (T_1-T_4)

Figure 5.13 : (a) Wall shear stress contour of coronary arteries important time step of cardiac cycle i.e. during (T_1-T_4), (b) during (T_4-T_8).

5.3.4 Oscillatory Shear Index (OSI)

The Oscillatory Shear Index, or OSI, is a hemodynamic statistic linked to flow oscillation that indicates the total WSS vector oscillation during the cardiac cycle relative to its mean direction. During the course of the cardiac cycle, the oscillation strength index (OSI) of vascular flows fluctuates between 0 and 0.5. Values of 0 and 0.5, respectively, designate regions with no reversal and a purely high oscillatory character of the flow. Values in the middle range, 0.1, indicate regions with a moderate oscillatory nature of the flow. In regions of the body with a lot of oscillatory flow, thrombosis tends to form and develop over time. Figure 5.14 depicts distribution of OSI. In Figure 5.14 (a) the highest OSI zones are indicated with a rectangular shape red & blue box. Figure 5.14 (b-e), shows the OSI distribution in the magnified view of lateral and anterior lateral position.

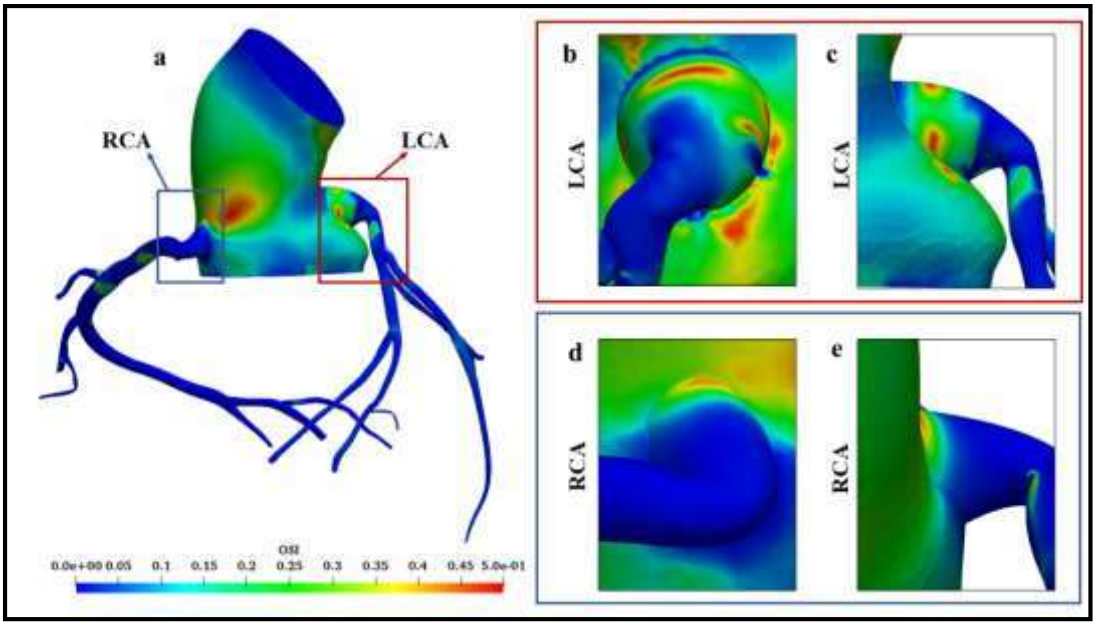

Figure 5.14 : Oscillatory Shear index (OSI) distribution contour map on vessel wall of (a) 3D model including LCA & RCA (b) magnified view of lateral LCA (c) magnified view of anterior lateral LCA (d) magnified view of lateral RCA (e) magnified view of anterior lateral RCA.

5.3.5 Time average wall shear stress (TAWSS)

WSS measures have shown potential in the investigation of atherosclerosis and plaque development because WSS has a big effect on the structure of the inner layer of the vessel wall. Blood flow models often use a number of WSS indices, like the TAWSS and the OSI, to describe the WSS as a single regional distribution. (Figure 5.15) shows both the lateral and anterior lateral view of the TAWSS distribution. The TAWSS is highest at the start of the RCA wall, the start of the LCA bifurcations, the RCA wall outlet (2–5), and the LCA walls outlet (1–3) and (6), with values greater than 75 Pa. This is because the sizes of those smaller vessels are getting smaller, which makes the flow speed go up and raises the TAWSS. TAWSS is also lower since the dimension of

the aorta, RCA, and LCA is bigger. Figure 5.3.5 (b-e), shows the TAWSS distribution in the magnified view of lateral and anterior lateral position.

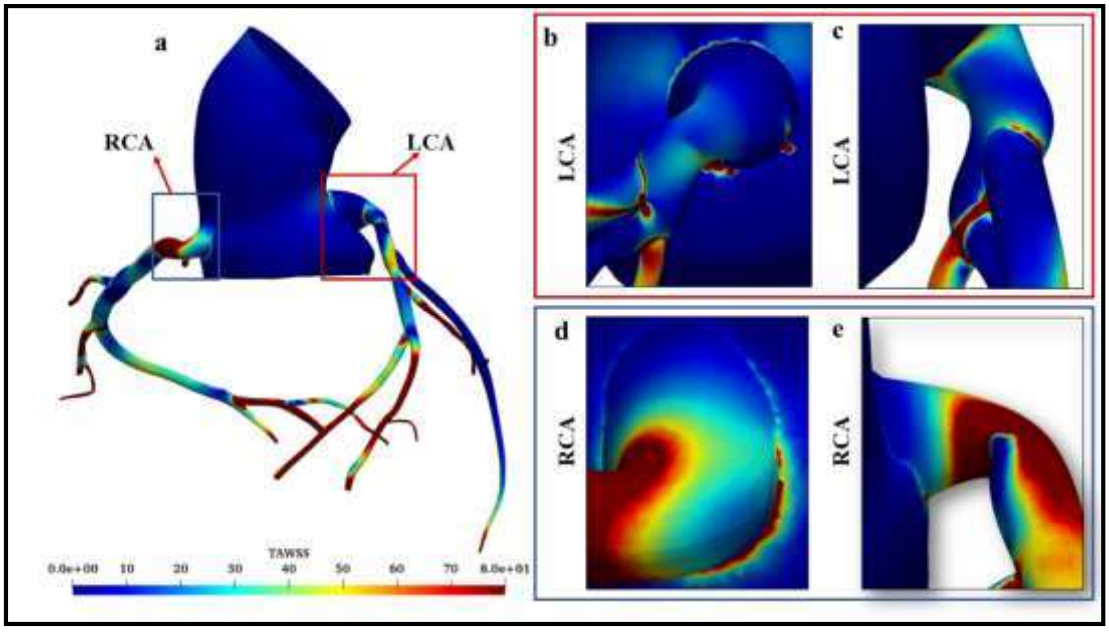

Figure 5.15 : Time average wall shear stress (TAWSS) a) 3D model including LCA & RCA (b) magnified view of lateral LCA (c) magnified view of anterior lateral LCA (d) magnified view of lateral RCA (e) magnified view of anterior lateral RCA.

5.3.6 Relative Residence Time (RRT) distribution

The RRT is a significant hemodynamic parameter that incorporates TAWSS and OSI effects. The RRT serves to measure the fluid's relative residence time in a particular area. The RRT also estimates the extent of penetration of macromolecules to subendothelial surfaces. (Figure 5.16 (a) & (b)) depicts typical RRT contours of a patient-specific coronary artery network with a curved shape. In regions with minimal TAWSS, the RRT of vascular blood flow through the arterial system reaches a high value. High RRT values appear in the aortic inlet and marked region with red box in (Figure 5.16). The elevated distribution of RRT expresses a description of TAWSS and

is useful for identifying and localizing both oscillating and low shear stresses. Therefore, RRT is a potential biomarker for locating prospective atherosclerosis-prone regions.

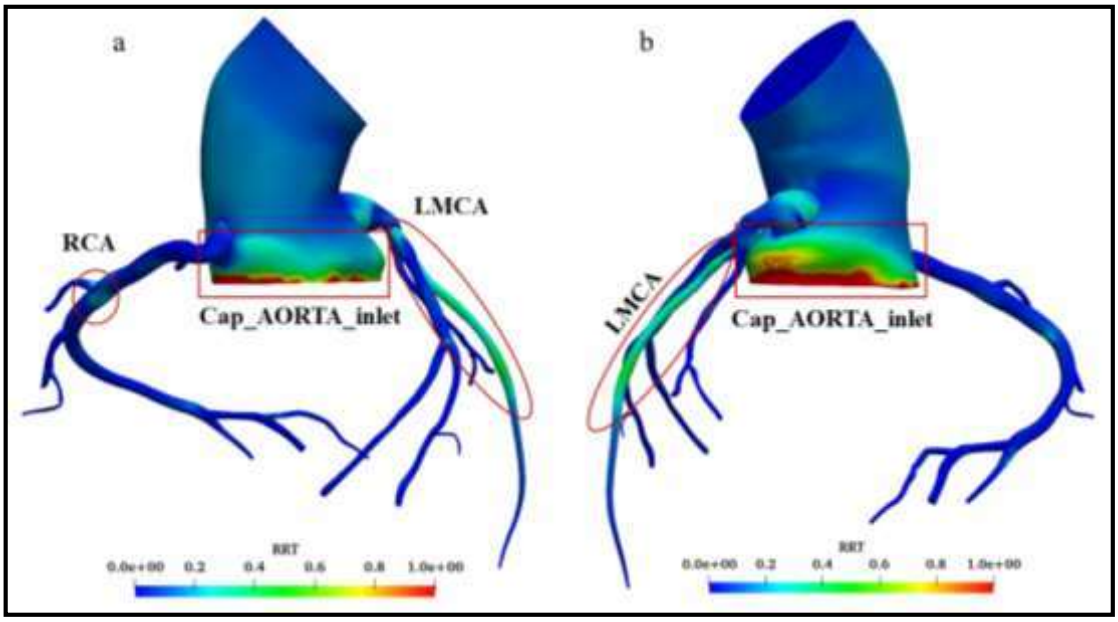

Figure 5.16 : Relative Residence Time (RRT) distribution (a) Anterior view, critical region marked with dark red outline (b) Posterior view and critical region marked with dark red outline.

5.4 Discussion

We successfully built and implemented a coronary boundary condition that relates a lumped parameter coronary vascular simulation to each coronary outlet of the three-dimensional finite element model of the aorta and epicardial coronary arteries. When attempting to depict the intramyocardial pressure by considering the interactions between the artery system, we used both a lumped parameter model, an open loop model, and an inflow boundary condition linking the two. Using this modeling technique, we investigated the effect of changes in cardiac and vascular characteristics

on coronary hemodynamics. It is difficult to predict if adverse events would occur in patients categorized as CAD-RADS system based on information supplied by CCTA on their first visit. The present investigation included a patient with probable coronary heart disease. CFD analysis was utilized to investigate the patient-specific hemodynamic features, which may give important information for diagnosis and therapy.

From Figure. 5.10 (a) & 5.11 (a) displayed no physiological features of the LCA and RCA flow waveforms. From Figure 5.15, it is noted that one-half of the vessel wall areas of the LCA and RCA had modest and high TAWSS values, respectively. Also, at the LMCA and LCA_1, large regions of low TAWSS (4 dynes/cm^2) and sluggish blood flow (close to stagnation) were observed. TAWSS > 40 dyne/cm^2 was present in the vessel walls of the middle and distal RCA and LCA. Previous research showed that TAWSS > 40 dyne/cm^2 or elevated OSI (no exact value but generally > 0.2 or 0.3) cause vascular wall damage, whereas TAWSS 4 dyne/cm^2 and blood flow disorder can cause extensive platelet aggregation, endothelial cell damage, and thrombosis and atherosclerosis (Park et al., 2016; Sanderson, 1992). Increased flow velocity may have caused more vascular wall damage in the patient's RCA and other left coronary branches, leading to a future readmission for coronary heart disease. Previous research has mostly focused on the stenoses' local hemodynamic anomalies (Liu et al., 2017; Malota et al., 2018). However, the current research reveals that overall hemodynamics (over the whole vessel) are equally deserving of attention, particularly in patients identified as potential patients for coronary artery disease who also present with chest discomfort. There is reason to suppose that this unusual hemodynamic environment

would result in plaque development and arterial wall damage if prompt therapy were not provided. Thus, at the first diagnosis, it is necessary to assess both local and general hemodynamics, as they may have a significant impact on clinical outcomes.

Although the sample size was limited in this research, findings such as hemodynamics over an entire vessel are of reference value in patients categorized as suspected patient coronary artery with chest pain at the time of their first visit. Our future studies will be based on the following early findings: (1) Would the severity of coronary stenosis possess a significant impact on coronary blood supply but a little impact on blood flow disorder? (2) Does the stenosis's location significantly impact the intraluminal blood flow disorder? (3) Can similar vascular bed shapes result in different clinical outcomes owing to hemodynamic differences? (4) To acquire more compelling findings, additional patient-specific measures, such as patient-specific intake flow rate waveform, should be employed.

Our methodology has few restrictions. As if we hadn't considered the heart's motion during the cardiac cycle. We affixed the coronary arteries to the epicardial region of the heart, as well as the surface in space and time. In reality, the heart contracts and relaxes significantly during the cardiac cycle. This movement is too large to be modelled using the coupled momentum technique, which is a linearized method employing a fixed fluid mesh. However, previous research demonstrated that the effects of cardiac movement were secondary and did not influence the pressure and flow fields as much as geometry and boundary conditions (Qiu and Tarbell, 2000; Ramaswamy et al., 2004; Santamarina et al., 1998; Zeng et al., 2008). We have

considered rigid boundary conditions on the wall, and fluid structure interaction can be solved with wall deformation movement information.

5.5 Summary

Using CFD methodologies, the present research carried out numerical simulations of patient-specific coronary models. We used a method known as (0D-3D) open loop modelling for the simulation. It is challenging to make an accurate diagnosis of a patient and choose an appropriate therapy for them just based on the data that was observed using CCTA. This open loop modelling approach with lumped parameter-based physiologically and geometrically realistic outflow pressures will help cardiologists to analyze medically imaged coronary arteries and compute hemodynamic parameters to assess their patients' risk of coronary arterial disease (CAD). In conclusion, patient-specific CFD analysis can be helpful in early diagnosis and therapy, particularly for individuals who might have coronary artery disease.